ROTATIONALLY STATE-SELECTED HBr^+: PREPARATION AND CHARACTERIZATION

Jinchun XIE and Richard N. ZARE
Department of Chemistry, Stanford University, Stanford, CA 94305, USA

Received 15 May 1989

Rotationally state-selected HBr^+ ions have been prepared by 2+1 resonance-enhanced multiphoton ionization (REMPI) via Rydberg states of HBr, and characterized by laser-induced fluorescence (LIF) using the HBr^+ $A\,^2\Sigma^+$–$X\,^2\Pi$ system. The experiment has been conducted under bulb conditions of 10–50 mTorr. The rotationally unrelaxed distribution of HBr^+ internal states shows that the ionization step can be highly selective, depending on the intermediate Rydberg state chosen.

1. Introduction

Consider the process

$$AB(v, J) + h\nu \rightarrow AB^+(v^+, J^+) + e^- \qquad (1)$$

in which the molecule AB in the rovibrational level (v, J) is photoionized to produce the molecular ion AB^+. A fundamental question is, what is the internal state distribution of the AB^+ ion; that is, which rovibrational levels (v^+, J^+) are populated by the photoionization process and to what extent? The answer to this question is not only important for understanding the dynamics of molecular photoionization [1–5] but also for preparing reagent ions in a state selective manner for subsequent study of their reactive and nonreactive collision dynamics [6–10].

In general, previous one-photon photoionization studies have not been able to determine the rotational distribution of the resulting molecular ion. There are two causes for this failure. First, there is the difficulty of isolating for study a single rovibrational level of the AB molecule. Often, the AB molecules in a sample are at thermal equilibrium and even at low temperature a fair number of (v, J) levels are occupied. Second, it is difficult to resolve the various (v^+, J^+) levels produced in the photoionization process. A method must be found for probing the internal state distribution of the nascent ion.

The first difficulty may be overcome by using $n+1$ resonance-enhanced multiphoton ionization (REMPI) [11,12]. Here the n-photon absorption step causes a bound–bound transition

$$AB(v, J) + nh\nu \rightarrow AB^*(v', J') \qquad (2)$$

in which the (v', J') rovibrational level of the electronically excited AB^* molecule is selected by the resonance condition $E[AB^*(v', J')] - E[AB(v, J)] = nh\nu$. This step is followed by a one-photon bound–free transition

$$AB^*(v', J') + h\nu \rightarrow AB^+(v^+, J^+) + e^- . \qquad (3)$$

It still remains to determine the (v^+, J^+) population distribution of the AB^+ ion.

One possibility is to use high-resolution photoelectron spectroscopy (PES). For H_2 this procedure is facilitated by the large energy spacings between rotational levels of the H_2^+ ion, and several rotationally selective REMPI–PES studies have been carried out [13,14]. For other molecules, photoelectron spectroscopy seldom has sufficient resolution. A notable exception is the REMPI–PES of NO, in which the final rotational distribution of the NO^+ ion can be extracted by measuring zero kinetic energy photoelectrons [15,16] or by recording the time-of-flight distribution of photoelectrons arising from the photoionization of high J levels [17–19]. An example of the latter technique is the study by Allendorf et al. [19], who observed the $\Delta N = 0, \pm 1$, and ± 2 transitions for high J levels ($J = 22.5$) of NO^+ $X\,^1\Sigma^+$ $v = 0$ in which the ionization proceeds through the $v = 0$ level of the NO $A\,^2\Sigma^+$ Rydberg state.

0 009-2614/89/$ 03.50

Another possibility is to probe the AB^+ ion by laser-induced fluorescence (LIF). The first REMPI–LIF experiment has already been demonstrated on CO under beam conditions [20]. Unfortunately, no significant rotational selection of the CO^+ ion resulted because the CO $B\,^1\Sigma^+$ intermediate state was not rotationally selected by the 2+1 REMPI process via the Q branch transitions (which form a bandhead). There has also been a REMPI–LIF study of N_2 in a static gas [21,22]. However, the low ion yield required this experiment to be carried out in N_2 samples at a pressure of 1–3 Torr. We report here a REMPI–LIF study of HBr with static gas at pressures of 10–50 mTorr. Under these conditions we can be confident that we can measure the $HBr^+(v^+, J^+)$ internal state distribution in the absence of collisional relaxation.

2. Experimental

Hydrogen bromide (99.95% pure, Matheson) slowly flows through a stainless steel chamber at a pressure of 10–50 mTorr. The chamber has long baffle arms with Brewster angle windows to reduce scattered laser light. The inside of the chamber is sprayed with flat black paint (ZC Black 200, Zuel Co.). This reduces the background scattered light by one to two orders of magnitude. When the HBr flow is turned off, the background pressure is 1×10^{-7} Torr. The output of the ionization laser is 0.5–2 mJ over the range 270–259 nm. This radiation is generated by frequency doubling the output of a coumarin 500 dye laser (PDL-1, Quanta-Ray) pumped by a pulsed Nd:YAG laser (DCR-1, Quanta-Ray). The ionization laser beam is focused in the center of the chamber with a 750 mm focal length lens. This loose focus increases the ionization volume while decreasing the effect of saturation. We have carried out 2+1 REMPI of HBr via its Rydberg states in the energy range 75200–78500 cm^{-1}. We show that it is possible to select the fine structure level of HBr^+ $X\,^2\Pi_{1/2,3/2}$ based on which HBr Rydberg state is accessed.

The HBr^+ $A\,^2\Sigma^+$–$X\,^2\Pi$ system is analogous to the OH $A\,^2\Sigma^+$–$X\,^2\Pi$ system and covers the wavelength range 330–360 nm. Emission from the HBr^+ A state was first observed in 1935 in discharges of HBr [23], and the HBr^+ A–X system has been subsequently analyzed in detail [24,25]. LIF has already been used to measure the HBr^+ A state radiative lifetime, which is about 3.9 μs [26]. This long lifetime allows us to avoid scattered light by delaying the measurement of fluorescence with respect to the time of pulsed laser excitation. In this regard, the HBr^+ system is rather ideal for study by LIF. Such measurements provide much detail concerning the $HBr^+(v^+, J^+)$ distribution, including even the relative population of the Λ-doublets (Ω-doublets).

The probe laser beam enters the chamber counterpropagating to the ionization laser beam. The probe laser beam is unfocused; it is 5 mm in diameter and has a power of 50–80 μJ per pulse. Under these conditions the HBr^+ LIF signal is observed to be linear with probe laser power. The (1, 0) HBr^+ $A\,^2\Sigma^+$–$X\,^2\Pi_{3/2}$ sub-band occurs at 330 nm and the (1, 0) HBr^+ $A\,^2\Sigma^+$–$X\,^2\Pi_{1/2}$ sub-band at 360 nm. The former wavelength is reached by doubling the output of a DCM dye laser and the latter by Raman shifting the doubled output from a rhodamine 575 dye laser. In each case the dye laser (PDL-1, Quanta-Ray) is pumped by a Nd:YAG laser (DCR-1, Quanta-Ray).

A pair of plates is located in the ionization region inside the gas chamber. The orientation of these plates is parallel to the two laser beams, and there is a 100 V potential between these plates. The ion signal from the plates is detected directly by a boxcar integrator (model 165, Princeton Applied Research) at the level of 50–1000 mV without the use of a preamplifier. This ion signal is used to tune the ionization laser output to various two-photon resonances in HBr. The applied voltage across these plates is then switched off during fluorescence measurements.

A collecting lens system (f1, quartz) is placed inside the chamber. It focuses fluorescence on a photomultiplier tube through a narrow band interference filter (10 nm fwhm, centered at 330 nm). The LIF signal is integrated for 2 μs with a CAMAC LeCroy 2249SG-ADC charge integrator whose opening is delayed by 1 μs from the firing of the ionization laser. The LIF laser output is delayed with respect to the ionization laser output by only 10 ns. Data are collected and analyzed on an IBM PC/XT personal computer.

3. Results and discussion

3.1. Appearance of the HBr^+ A–X spectrum

Fig. 1 shows a laser excitation spectrum of the (1, 0) band of the $HBr^+ A\,^2\Sigma^+ - X\,^2\Pi_{1/2}$ system. The HBr^+ ions are produced by 2+1 REMPI via the $v=0$, $J=4$ level (e Λ-component of + parity) of the HBr $F\,^1\Delta_2$ state as the intermediate state (S(2) line). The HBr $F\,^1\Delta_2$ Rydberg state is a good choice for 2+1 REMPI because the two-photon transitions to levels of this state are strong and sharp, resulting in a large ion yield. Consequently, the LIF spectrum (fig. 1) has excellent signal to noise.

The experimental conditions for this spectrum are 22 mTorr of HBr and a 10 ns delay between ion formation and ion excitation. When the sample pressure is increased to 50 mTorr and the delay lengthened to 50 ns, this spectrum has almost the same appearance. Therefore, we conclude that the present spectrum is representative of the nascent HBr^+ distribution, that is, the HBr^+ ions are not collisionally relaxed.

Examination of fig. 1 shows the six branches characteristic of a $^2\Sigma^+ - ^2\Pi_{1/2}$ electronic transition. Fig. 2 presents a Herzberg diagram indicating the relevant transitions occurring between the HBr $X\,^1\Sigma^+$ state, the HBr $F\,^1\Delta_2$ state, the HBr^+ $X\,^2\Pi_{1/2}$ state, and the HBr^+ $A\,^2\Sigma^+$ state. Spin–orbit interaction causes the HBr^+ $X\,^2\Pi$ state to be split into two sub-states, $X\,^2\Pi_{3/2}$ and $X\,^2\Pi_{1/2}$, which are separated by over 2500 cm^{-1} with the $X\,^2\Pi_{3/2}$ state lying lower (inverted splitting). Because of this large spin–orbit interaction, HBr^+ closely follows Hund's case (c) coupling. The HBr^+ $A\,^2\Sigma^+$ state also has an unusually large spin–rotation splitting ($\gamma_e=2.10\ cm^{-1}$), which causes the R_{12} and Q_2 branch members as well as the Q_{12} and P_2 branch members with the same J to be resolved.

The HBr^+ $A\,^2\Sigma^+ - X\,^2\Pi_{1/2}$ system behaves as a $(1/2)\leftrightarrow(1/2)$ transition in Hund's case (c) coupling. Therefore, the rotational line strengths are given by the expressions [27] shown in table 1. They involve the parallel and perpendicular components of the transition dipole moment, denoted by $\mu_\parallel$ and $\mu_\perp$, respectively. These have the normalization property that

$$|\mu_\parallel|+|\mu_\perp|=1\,. \tag{4}$$

For the HBr^+ A–X band system, the values of $\mu_\parallel$ and

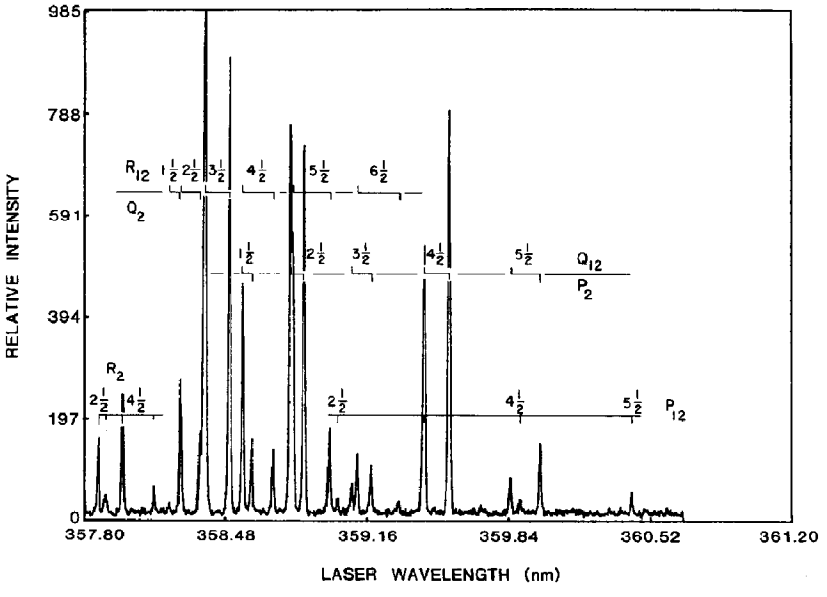

Fig. 1. LIF spectrum of the (1, 0) band of the HBr^+ $A\,^2\Sigma^+ - X\,^2\Pi_{1/2}$ system. The HBr^+ is formed by 2+1 REMPI via the $F\,^1\Delta_2$ $v=0$, $J=4$ level (S(2) transition). The HBr sample pressure is 22 mTorr.

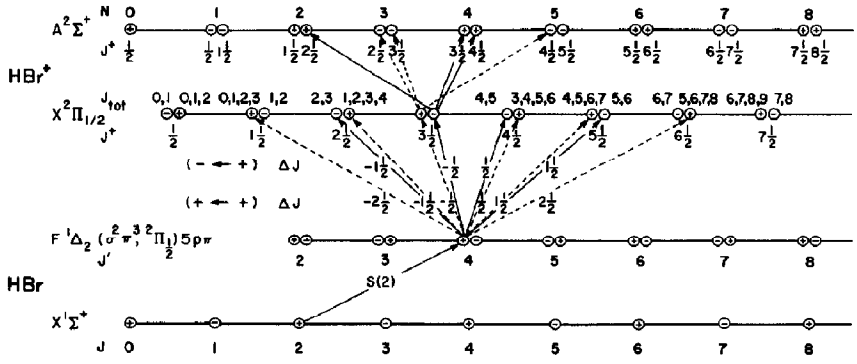

Fig. 2. Herzberg diagram for the HBr^+ REMPI–LIF process corresponding to the spectrum shown in fig. 1.

$\mu_\perp$ are not known, but from the strengths of the different branches it appears that $\mu_\parallel$ and $\mu_\perp$ are comparable in magnitude and have the same sign. This causes members of the P_{12} and R_2 branches to be very weak owing to the common $\mu_\parallel - \mu_\perp$ factor in the expression for the rotational line strengths (see table 1). Conversely, the members of the P_2 and R_{12} branches are strong. Note that these two branches arise from Λ components (Ω components) of opposite parity (see fig. 2). They both have the common factor, $\mu_\parallel + \mu_\perp$ (see table 1). Therefore, they are ideal branches for quantifying the relative population of rotational levels in the two Λ components (Ω components) of the HBr^+ $X\,^2\Pi_{1/2}$ ground state.

Table 1
Rotational line strengths [a] for a $^2\Sigma^+ - ^2\Pi_{1/2}$ transition in Hund's case (c)

Branch	Line strength
$P_{12}(J)$	$\frac{(J+1/2)(J-1/2)}{J}(\mu_\parallel-\mu_\perp)^2$
$P_2(J)$	$\frac{(J+1/2)(J-1/2)}{J}(\mu_\parallel+\mu_\perp)^2$
$Q_{12}(J)$	$\frac{2(J+1/2)^3}{J(J+1)}\left(\frac{\mu_\parallel}{2J+1}+\mu_\perp\right)^2$
$Q_2(J)$	$\frac{2(J+1/2)^3}{J(J+1)}\left(\frac{\mu_\parallel}{2J+1}-\mu_\perp\right)^2$
$R_{12}(J)$	$\frac{(J+1/2)(J+3/2)}{J}(\mu_\parallel+\mu_\perp)^2$
$R_2(J)$	$\frac{(J+1/2)(J+3/2)}{J}(\mu_\parallel-\mu_\perp)^2$

[a] From ref. [27].

3.2. HBr^+ $X\,^2\Pi_{1/2}$ rotational distribution

Fig. 3 presents the relative rotational populations of the $v=0$ level of the HBr^+ $X\,^2\Pi_{1/2}$ state when the $v=0, J=4$ level ((+) parity component) of the HBr $F\,^1\Delta_2$ state is the intermediate state in 2+1 REMPI. These rotational populations are derived from the members of the P_2 and R_{12} branches of the LIF spectrum (see fig. 1) using the line strengths given in table 1. We have neglected any effect of alignment on the intermediate state [19] but we have corrected for the variation of LIF signal with the wavelength of the excitation laser. We see from fig. 3 that only a few rotational levels of the HBr^+ ion are populated by this 2+1 REMPI process. However, there is a preference for populating the Λ component (Ω component) of (−) parity.

To understand this result, we return to the Herz-

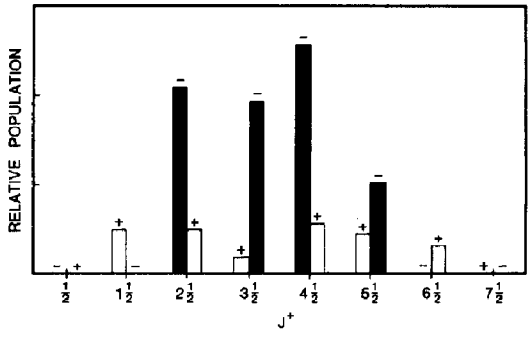

Fig. 3. Rotational population distribution for HBr^+ $X\,^2\Pi_{1/2}$ $v^+=0$. The + and − signs indicate the Λ-doublet (Ω-doublet) component of a J^+ rotational level.

berg diagram shown in fig. 2. The transitions between $HBr^+ X\,^2\Pi_{1/2}$ and HBr $F\,^1\Delta_2$ are indicated by a solid line for $(\pm)\leftrightarrow(\mp)$ and by a dashed line for $(\pm)\leftrightarrow(\pm)$. These lines connect various $\Delta J = J^+ - J'$ transitions originating from the HBr $F\,^1\Delta_2$ $J=4$ ((+) parity component) level. We conclude that there is a marked preference (propensity) for the transitions connected by solid lines, that is, for those transitions in which the parity changes. Studies of other J' levels of the HBr $F\,^1\Delta_2$ state show the same rotational population pattern of the $HBr^+ X\,^2\Pi_{1/2}$ state irrespective of how the intermediate level is pumped. When a J' level of (−) parity is pumped, then the pattern is the same except that the parities of the final rotational levels are reversed.

In Hund's case (c) coupling, the intermediate state (HBr $F\,^1\Delta_2$) and the final state ($HBr^+ X\,^2\Pi_{1/2}$) are represented by $|J'\Omega'M'\rangle$ and $|J^+\Omega^+M^+\rangle$. The photoelectron may be described in a coupled representation as $|j_e m_e\rangle$ [28], which may be transformed into the molecular frame by

$$|j_e m_e\rangle = \sum_{\omega_e} D^{j_e}_{m_e\omega_e}(R)\,|\omega_e\rangle\,, \tag{5}$$

where D is a Wigner rotation matrix element. The photoionization process involves an electric dipole transition between the intermediate state and the total final state $|J^+\Omega^+M^+\rangle|j_e m_e\rangle$. By making the initial and final states as eigenstates of the parity operator and by evaluating the electric dipole moment matrix element connecting them, we have deduced [29] the following selection rule:

$$J^+ - J' + j_e + p^+ + p' = \text{even}\,, \tag{6}$$

where p^+ and p' are the parities of the final ion state and the intermediate neutral state. In particular, $p=0$ for a level with e parity and $p=1$ for a level with f parity [30]. This selection rule for photoionization between two case (c) levels implies the following:

$$(\pm)\leftrightarrow(\mp)\quad j_e = 1/2, 5/2, 9/2, \ldots\,, \tag{7a}$$

$$(\pm)\leftrightarrow(\pm)\quad j_e = 3/2, 7/2, 11/2, \ldots\,. \tag{7b}$$

Thus, the photoelectron angular momentum can only be of two types, where $j_e - 1/2$ is even for $(\pm)\leftrightarrow(\mp)$ and odd for $(\pm)\leftrightarrow(\pm)$.

Consider transitions of the type $(\pm)\leftrightarrow(\mp)$, shown as solid lines in fig. 2. Examination of the observed levels indicates that $j_e = 1/2$ only, that is, $j_e = 5/2$, 9/2, etc., are not present. This can be seen from the value of J_{tot}, the total angular momentum quantum number, which is the result of coupling J^+ and j_e. Its value covers the range $J_{tot} = J^+ + j_e$, $J^+ + j_e - 1$, ..., $|J^+ - j_e|$. Fig. 2 shows that the only value of j_e is $j_e = 1/2$. This conclusion is reached by realizing that only for $j_e = 1/2$ does $\Delta J_{tot} = J_{tot} - J'$ take on the values of 0 and ±1. Similarly, examination of the $(\pm)\leftrightarrow(\pm)$ transition (dashed lines in fig. 2) shows that the value of j_e is restricted to $j_e = 3/2$. We conclude that photoionization from the HBr $F\,^1\Delta_2$ state is dominated by outgoing photoelectrons with angular momentum $j_e = 1/2$ and 3/2, with a strong preference for the former. Thus, the partial wave expansion of the photoelectrons is limited to two terms in this case, with the s-wave dominant.

3.3. HBr^+ $X\,^2\Pi$ fine structure distribution

Just as there is a preference for which J level and which parity component is populated in the HBr^+ ion, it might be expected that the $HBr^+ X\,^2\Pi_{1/2}$ and $X\,^2\Pi_{3/2}$ states are unequally populated. Indeed, this is clearly the case, as can be seen in fig. 4, which shows the LIF spectra from the two sub-bands. In this figure, the narrow band filter (centered at 330 nm) is the same for both sub-bands and the sub-bands are recorded at the same pressure and with the same ion yield. Moreover, the excitation has approximately the same intensity over both sub-bands. The emission spectrum from the $HBr^+ A\,^2\Sigma^+$ state to the $HBr^+ X\,^2\Pi_{3/2}$ and $X\,^2\Pi_{1/2}$ states has previously been shown by Okase, Tsuji, and Nishimura [31] to be of comparable strength. Consequently, the two spectra in fig. 4 can be compared directly. We conclude that more than 99% of the $HBr^+ X\,^2\Pi$ state has been selected as the $X\,^2\Pi_{1/2}$ component through 2+1 REMPI via the HBr $F\,^1\Delta_2$ state. This conclusion has also been confirmed independently by time-of-flight photoelectron spectroscopy [32]. This latter study has also shown that the $\Delta v = 0$ transition occurs almost exclusively in the photoionization step, as expected for a transition between a neutral Rydberg state and the ionic ground state [33–35].

A simple explanation may be offered for this striking preference to select the $HBr^+ X\,^2\Pi_{1/2}$ fine structure component when ionizing the HBr $F\,^1\Delta_2$ state.

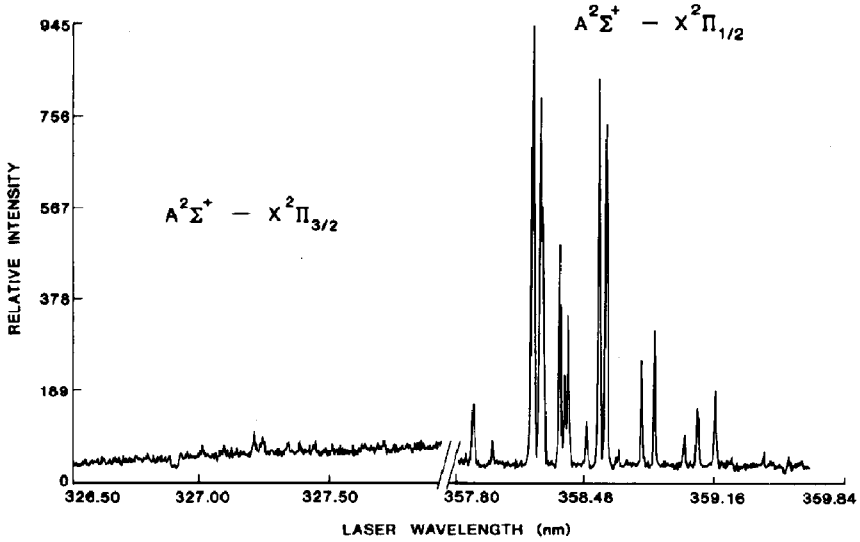

Fig. 4. LIF spectra of the (1, 0) band in HBr^+ $A\,^2\Sigma^+$–$X\,^2\Pi_{3/2}$ and $A\,^2\Sigma^+$–$X\,^2\Pi_{1/2}$ with the same laser power for both sub-bands. The HBr^+ is formed via the R(1) line of the HBr F–X transition with the same ion yield. The HBr sample pressure is 12 mTorr.

The electronic configuration of the HBr $F\,^1\Delta_2$ state is a $\sigma^2\pi^3\,^2\Pi_{1/2}$ core with a $5p\pi_{3/2}$ Rydberg electron. If photoionization causes the ejection of the Rydberg electron with no effect on the core, then the HBr^+ ion should be exclusively formed in the $X\,^2\Pi_{1/2}$ state, as is observed. We have further tested this hypothesis by examining the 2+1 REMPI of HBr via the HBr $f\,^3\Delta_2$ state. This intermediate state is described as a $^2\Pi_{3/2}$ core with a $5p\pi_{1/2}$ Rydberg electron. As anticipated, only $HBr^+\,^2\Pi_{3/2}$ ions are observed. This behavior offers the rare opportunity to prepare molecular ions by 2+1 REMPI in a highly state-selective manner. This may have much utility in the detailed study of ion–molecule collision processes.

Acknowledgement

This work was supported by the Air Force Office of Scientific Research under AFOSR 89-0264.

References

[1] K. Siegbahn, C. Nordling, G. Johansson, J. Hedman, P.F. Héden, K. Hamrin, U. Gelius, T. Bergmark, L.O. Werme, R. Manne and Y. Baer, ESCA applied to free molecules (North-Holland, Amsterdam, 1969).

[2] D.W. Turner, A.D. Baker, C. Baker and C.R. Brundle, Molecular photoelectron spectroscopy, a handbook of He 584 Å spectra (Interscience, New York, 1970).

[3] J.H.D. Eland, Photoelectron spectroscopy (Wiley–Halsted, New York, 1974).

[4] J.W. Rabalais, Principles of ultraviolet photoelectron spectroscopy (Wiley–Interscience, New York, 1977).

[5] J. Berkowitz, Photoabsorption, photoionization, and photoelectron spectroscopy (Academic Press, New York, 1979).

[6] W.A. Chupka, M.E. Russell and K. Rafaey, J. Chem. Phys. 48 (1968) 1518;.
W.A. Chupka and M.E. Russell, J. Chem. Phys. 48 (1968) 1527.

[7] S.L. Anderson, F.A. Houle, D. Gerlich and Y.T. Lee, J. Chem. Phys. 75 (1981) 2153;
T. Turner, O. Dutuit and Y.T. Lee, J. Chem. Phys. 81 (1984) 3475.

[8] R.J.S. Morrison, W.E. Conaway, T. Ebata and R.N. Zare, J. Chem. Phys. 84 (1986) 5527;
W.E. Conaway, T. Ebata and R.N. Zare, J. Chem. Phys. 87 (1987) 3447, 3453.

[9] C.Y. Ng, in: Techniques of chemistry, Vol. 20. Techniques for the study of ion–molecule reactions, eds. J.M. Farrar and W.H. Saunders (Wiley, New York, 1988) pp. 417–488.

[10] T.M. Orlando, B. Yang and S.L. Anderson, J. Chem. Phys. 90 (1989) 1577.

[11] D.H. Parker, in: Ultrasensitive laser spectroscopy, ed. D.S. Kliger (Academic Press, New York, 1983) p. 233.

[12] J.A. Syage and J.E. Wessel, Appl. Spectry. Rev. 24 (1988) 1.

[13] S.T. Pratt, P.M. Dehmer and J.L. Dehmer, J. Chem. Phys. 87 (1983) 4315.
[14] M.A. O'Halloran, S.T. Pratt, P.M. Dehmer and J.L. Dehmer, J. Chem. Phys. 87 (1987) 3288.
[15] K. Müller-Detlefs, M. Sander and E.W. Schlag, Chem. Phys. Letters 112 (1984) 291.
[16] M. Sander, L.A. Chewter, K. Müller-Detlefs and E.W. Schlag, Phys. Rev. A 36 (1987) 4543.
[17] W.G. Wilson, K.S. Viswanathan, E. Sekreta, E.R. Davidson and J.P. Reilly, J. Phys. Chem. 88 (1984) 672.
[18] K.S. Viswanathan, E. Sekreta, E.R. Davidson and J.P. Reilly, J. Phys. Chem. 90 (1986) 5978.
[19] S.W. Allendorf, D.J. Leahy, D.C. Jacobs and R.N. Zare, J. Chem. Phys., in press.
[20] L.F. Dimauro and T.A. Miller, Chem. Phys. Letters 138 (1987) 175.
[21] T. Ebata, A. Fujii and M. Ito, J. Phys. Chem. 91 (1987) 3125.
[22] A. Fujii, T. Ebata and M. Ito, J. Chem. Phys. 88 (1988) 5307.
[23] F. Norling, Z. Physik 95 (1935) 179; 106 (1936) 177.
[24] R.F. Barrow and A. Count, Proc. Phys. Soc. (London) A 66 (1953) 617.
[25] J. Lebreton, J. Chim. Phys. 70 (1973) 1188.
[26] C.C. Martner, J. Pfaff, N.H. Rosenbaum, A. O'Keefe and R.J. Saykally, J. Chem. Phys. 78 (1983) 7073.
[27] I. Kopp and J.T. Hougen, Can. J. Phys. 45 (1967) 2581.
[28] R.N. Zare, Angular momentum (Wiley, New York, 1988) pp. 232–236.
[29] J. Xie and R.N. Zare, unpublished results.
[30] J.M. Brown, J.T. Hougen, K.-P. Huber, J.W.C. Johns, I. Kopp, H. Lefebvre-Brion, A.J. Merer, D.A. Ramsay, J. Rostas and R.N. Zare, J. Mol. Spectry. 55 (1975) 500.
[31] H. Obase, M. Tsuji and Y. Nishimura, Chem. Phys. 99 (1985) 111.
[32] D.J. Leahy, J. Xie and R.N. Zare, unpublished results.
[33] J.T. Meek, S.R. Long and J.P. Reilly, J. Phys. Chem. 86 (1982) 2809.
[34] S.L. Anderson, D.M. Rider and R.N. Zare, Chem. Phys. Letters 93 (1982) 11.
[35] W.E. Conaway, R.J.S. Morrison and R.N. Zare, Chem. Phys. Letters 113 (1985) 429.